Origin of magnetic field-induced magnetic anisotropy in amorphous CoFeB thin films

Cite as: AIP Advances **12**, 045203 (2022); https://doi.org/10.1063/5.0086805
Submitted: 05 February 2022 • Accepted: 11 March 2022 • Published Online: 01 April 2022

Lu Yuan, Baomin Wang, Dezhi Zha, et al.

Origin of magnetic field-induced magnetic anisotropy in amorphous CoFeB thin films

Cite as: AIP Advances 12, 045203 (2022); doi: 10.1063/5.0086805
Submitted: 5 February 2022 • Accepted: 11 March 2022 •
Published Online: 1 April 2022

Lu Yuan,[1,2] Baomin Wang,[2,3,a)] Dezhi Zha,[2] Chenxu Liu,[4] Mengchao Li,[2] Yali Xie,[2] Huali Yang,[2] Yanwei Cao,[4] Hui Xu,[1,a)] and Run-Wei Li[2,5,a)]

AFFILIATIONS

[1] Institute of Materials Science, School of Materials Science and Engineering, Shanghai University, Shanghai 200072, People's Republic of China

[2] CAS Key Laboratory of Magnetic Materials and Devices and Key Laboratory of Magnetic Materials and Application Technology, Ningbo Institute of Materials Technology and Engineering, Chinese Academy of Sciences, Ningbo 315201, People's Republic of China

[3] School of Physical Science and Technology, Ningbo University, Ningbo 315211, People's Republic of China

[4] Laboratory of Advanced Nano Materials and Devices, Ningbo Institute of Materials Technology and Engineering, Chinese Academy of Sciences, Ningbo 315201, People's Republic of China

[5] Center of Materials Science and Optoelectronics Engineering, University of Chinese Academy of Sciences, Beijing 100049, People's Republic of China

[a)] **Authors to whom correspondence should be addressed:** wangbaomin@nimte.ac.cn; huixu8888@shu.edu.cn; and runweili@nimte.ac.cn

ABSTRACT

Magnetic anisotropy (MA) is an important property of magnetic materials, which not only determines the orientation of the magnetic moment in the magnetic material but also influences the working frequency of magnetoelectric devices. Unrevealing the origin of MA has become an important topic and attracts lasting interest. Here, we report a quite significant magnetic field-induced uniaxial MA in amorphous CoFeB thin films containing double ferromagnetic atoms. The thickness independence of MA was obtained by observing a series of hysteresis loops and magnetic domains. The MA is proved subtly to be related to the variation of orbital magnetic moment acquired by ferromagnetic resonance. Furthermore, we found that atoms combine into clusters and incline to an order in amorphous CoFeB thin films with field-induced MA. Based on these experimental results, we proposed a direction-like order model to interpret the origin of magnetic field-induced MA in amorphous CoFeB thin films well.

When the orientation of the magnetic moment has a prominent effect on the total energy of ferromagnetic material, it signifies the appearance of the phenomenon of magnetic anisotropy (MA). As MA affects the working frequency and transport capacity of magnetoelectric devices, it is essential for researchers to regulate MA in many important fields, such as information storage, biomedicine, and geomagnetic detection.[1–5] The magnetic anisotropy originates from multifarious sources such as magnetocrystalline anisotropy, shape anisotropy, exchange anisotropy, anisotropy induced by the magnetic field, and so on. Up until now, the origin of MA, as a momentous subject, has attracted intensive interest. In general, unlike the exchange interaction originated from electronic spin, which has the isotropic property, the orbital moment's anisotropy is very important for MA of the crystalline material. Concretely, it relies on spin–orbital coupling interaction of the ferromagnetic material and can interact with atomic structure and spin magnetization.[6–13]

With regard to the anisotropy of the amorphous material induced by the magnetic field, which attracted lasting interest, some works have certified that the local structural anisotropy or spin reorientation explains this phenomenon in thin films that contain only a type of ferromagnetic (Co, Fe, or Ni) and other non-ferromagnetic atoms.[14–16] The work of Chen *et al.*[17] further indicated that the surface-induced short-range order is the origin

of MA for amorphous transition metal rare earth films deposited in a magnetic field. However, for the magnetic thin films containing different types of ferromagnetic atoms such as amorphous Co–Fe–B films, which have wide applications such as magnetic random access memory (MRAM),[18,19] the origin of magnetic field-induced MA has not been fully identified.[20–22] In this work, we selected amorphous $Co_{40}Fe_{40}B_{20}$ (CoFeB) thin film as representative materials to investigate the mechanism of magnetic field-induced MA in the thin film containing two types of ferromagnetic atoms. Based on a number of experimental characterization and analyzing the change of structure or magnetic moment in these films, we proposed a direction-like order model to explain in-plane MA induced by magnetic field in the amorphous CoFeB thin film.

A series of Ta (2 nm)/CoFeB (10, 30, 50, 150, and 250 nm) films were grown on a Si substrate at room temperature by dc magnetron sputtering without magnetic field (OMF-CoFeB) and with 800 Oe magnetic field (MF-CoFeB). The vacuum of the sputtering

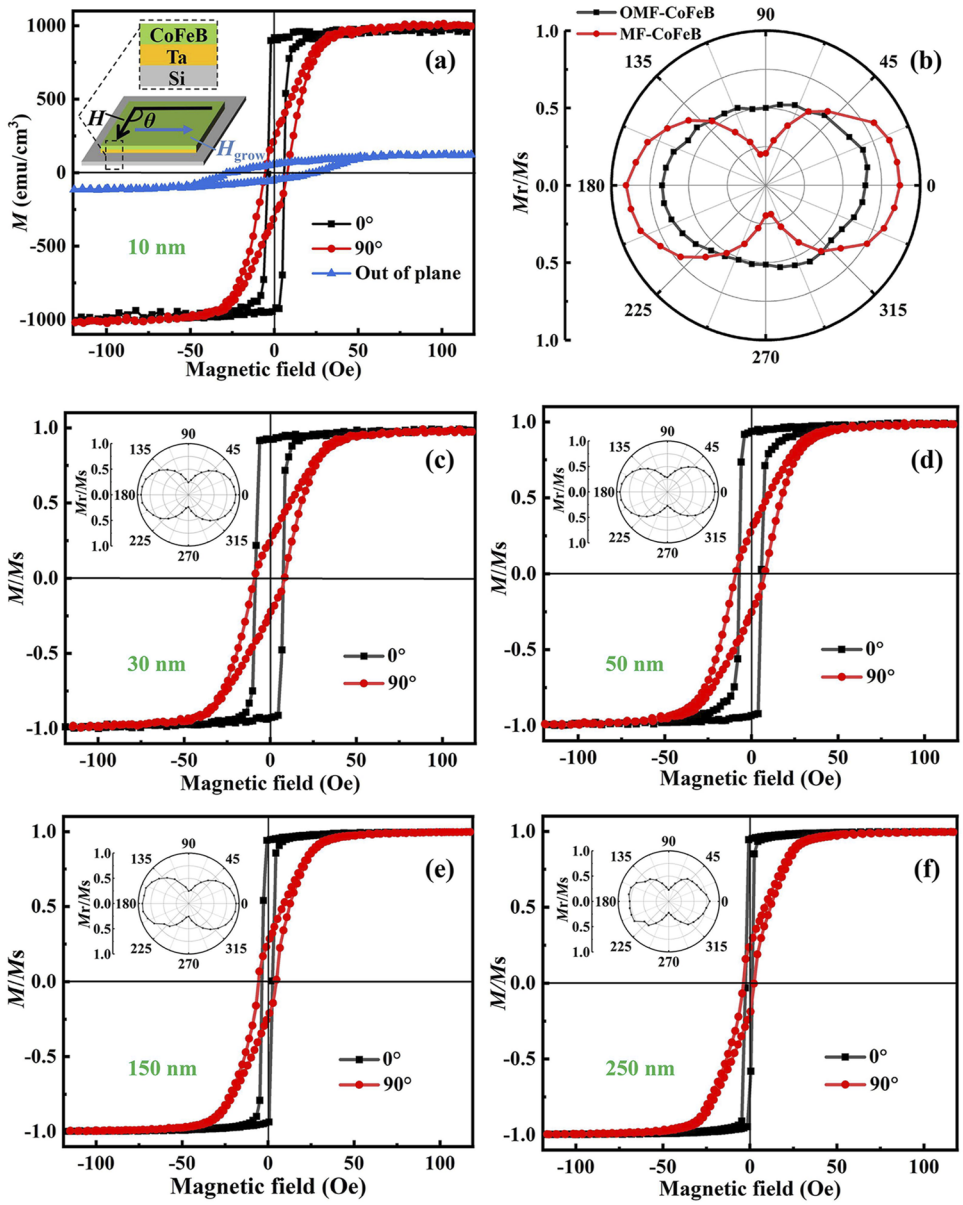

FIG. 1. (a) Hysteresis loops of 10 nm CoFeB/Ta/Si. The insets show the experimental setup of VSM characterization. (b) Angular dependence of normalized M_r/M_s for 10 nm CoFeB/Ta/Si. Hysteresis loops for (c) 30 nm, (d) 50 nm, (e) 150 nm, and (f) 250 nm CoFeB/Ta/Si, and corresponding insets exhibit the angular dependence of normalized M_r/M_s.

chamber could be below 2.1×10^{-6} Pa as the base pressure. During the deposition, we maintained the the rotation rate of the sample stage at 10 rpm to greatly weaken the influence of oblique sputtering on the MA[23] and the pressure of Ar at 1.3 Pa. At the same time, the flowing rate of Ar and deposition power were 25 SCCM and 80 W, respectively. It is noted that there was ~2 nm Ta deposited as the buffer layer before growing CoFeB film. Then, the surface morphology of these specimens was observed by atomic force microscopy (AFM, Bruker Dimension Icon), and the magnetic domains were observed by magnetic force microscopy (MFM). By using a vibrating sample magnetometer (VSM, Lakeshore 7410), we obtained the angular dependence of hysteresis loops at room temperature. Here, the film was placed on a flat tail in a fused silica sample rod to rotate, where the direction of the external magnetic field H was parallel to the sample plane. The schematic diagram of the sample layout is depicted in the inset of Fig. 1(a). The dynamic magnetic characterization was carried out by ferromagnetic resonance (FMR) at electron spin resonance spectrometer (ESR, E500), which operated at a resonance frequency of $f_r = 9.8$ GHz. In addition, the film surface structure was confirmed from transmission electron microscopy (TEM, Tecnai F20) images.

Figure 1(a) shows hysteresis loops with different thicknesses and angular dependence of squareness M_r/M_s obtained by VSM. On the one hand, when the applied magnetic field H increased to 150 Oe, along with different directions, a different magnetic field strength is required for the magnetic moments to attain saturation. On the other hand, the curvilinear shape of the angular dependence of M_r/M_s tended to be ellipse shape for OMF-CoFeB; however, it becomes an "8" shape for MF-CoFeB [Fig. 1(b)]. The MF-CoFeB thin film shows more significant in-plane uniaxial MA than that of OMF-CoFeB film.[21,24] Here, the small in-plane anisotropy of OMF-CoFeB may be due to the effect of the stray field.[25,31] Then, considering the influence of CoFeB thickness, we measured a number of hysteresis loops with different CoFeB thicknesses, as shown in Figs. 1(c)–1(f). We can observe that the direction of H_{grow} corresponds to the easy axis. Furthermore, these curves of the angular dependence of M_r/M_s are still "8" shape with thickness from 10 to 250 nm, although this "8" becomes smaller and more irregular with 250 nm CoFeB. That is, the in-plane MA decreases obviously when the thickness of the CoFeB film increases to 250 nm. Meanwhile, the coercivity H_c changes in the range of 2.0–11.4 Oe.

Figures 2(a)–2(d) show a series of surface topographies with different CoFeB films from 10 to 250 nm. Here, these AFM images were obtained with a scanning area of 3×3 μm^2. Regardless of the changes in the CoFeB thickness, all these films have a very flat surface, which fluctuates around the root-mean-square roughness (R_q) of 0.2 nm when the thickness is less than 40 nm and then slightly increases along with the increase in the film thickness (only arrived in R_q 0.5 nm with 250 nm CoFeB). The result indicates that the quality of these films was outstanding. The corresponding magnetic domains are shown in Figs. 2(e)–2(h). Here, the color scale for Figs. 2(e)–2(h) is the phase change of the magnetic probe caused by long-range magnetic force, which reflects the magnitude of out-of-plane magnetization in the thin film. It is unusual that there has been a stripe structure in the magnetic domain with 250 nm CoFeB. By combining with the results of previous works,[26] we can infer that this is because a number of columnar crystals appear in the base of amorphous CoFeB (~200 nm), which destroy the original microstructure and decrease the MA. In short, amorphous MF-CoFeB films show a significant in-plane uniaxial MA, and this MA still remained outstanding when the CoFeB thickness lies between 10 and 250 nm.

To confirm the magnetic field-induced MA in amorphous CoFeB film, we perform a deep analysis by using FMR. In general, the FMR technology can be used to determine the MA and Landé g factor related to the spin and orbital magnetic moments. According to the work of Gayen *et al.*,[27] when $\mu_0 M_s \gg H_k$, the expression of the in-plane FMR resonance field (H_r) can be simplified to

$$\mu_0 H_r = H_0 - H_k \cos 2\varphi_H, \tag{1}$$

where M_s is the saturation magnetization, H_k is the anisotropy field associated with the in-plane uniaxial anisotropy constant K_u ($= H_k M_s/2$), and H_0 is the order of $(2\pi f_r/\gamma)^2/\mu_0 M_s$, where γ ($=g\mu_B/\hbar$) represents the gyromagnetic ratio related to the g factor, the reduced Planck constant ($\hbar$), and Bohr magneton (μ_B). We can obtain H_k by fitting the curve of the in-plane angular dependence of H_r. Figures 3(a) and 3(b) show a polar coordinate system of the

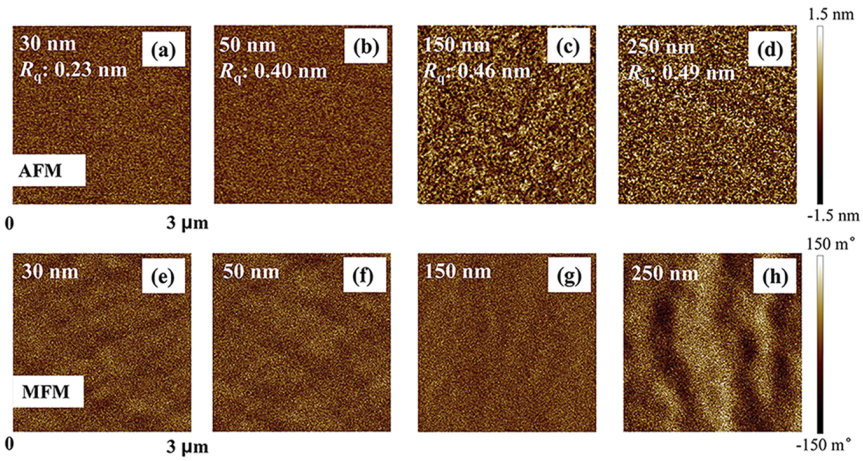

FIG. 2. (a)–(d) The AFM images (with R_q) and (e)–(h) the corresponding MFM images of CoFeB films grown on the Si substrates with different thicknesses.

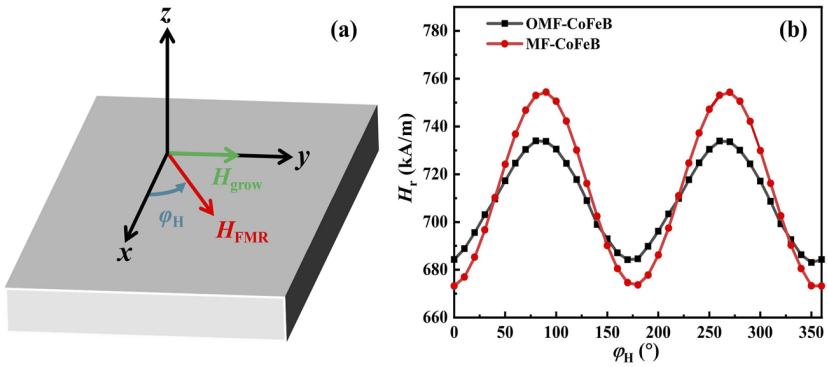

FIG. 3. (a) Schematic diagram of H_{FMR} in a spherical polar coordinate system. φ_H is the in-plane angle of the external magnetic field H_{FMR} to the *x* axis. (b) In-plane angular independence of resonance field (H_r) for near 30 nm CoFeB films.

sample configuration used in the subsequent discussion and an in-plane angular dependence of FMR resonance fields with 30 nm CoFeB film. It is noted that the dc external magnetic field H_{FMR} in the horizontal plane is perpendicular to the direction of the easy magnetic axis (H_{grow}) when φ_H was 0° as depicted in Fig. 3(a). The in-plane angular dependence of H_r is shown in Fig. 3(b), and the solid line represents the corresponding simulated result by using Eq. (1). It is clear that H_r (φ_H) had a periodic variation with cycle 180° and could be fitted well by using Eq. (1). Therefore, we can obtain the values of M_s, H_k, and K_u. It is noted that M_s slightly decreases from 88.7 Oe at OMF-CoFeB to 83.5 Oe at MF-CoFeB, and H_k and K_u increase from 23.2 to 50.0 Oe and from 0.8×10^3 to 1.7×10^3 J/m^3, respectively. In addition, the M-H loops of 30 nm CoFeB are shown in Fig. 1(c), combined with $H_k = H_{sat}(0°) - H_{sat}(90°)$;[31] thus, the value of H_k is about 49 Oe. Therefore, all these observations are in line with the VSM results depicted in Fig. 1, and the applied magnetic field, indeed, induces MA significantly.

In addition, the *g* factor can be used to investigate the change in the magnetic moment. We obtained γ and *g* factor deduced by Eq. (1) in the order of 2.01×10^{11}/(sT) and 2.29, respectively. Then, by simply considering Larmor motion condition,[28,29]

$$w_0 = \gamma H_r. \tag{2}$$

We found that the value of γ is 8.71×10^{11}/(sT), which is also in the order of the one deduced by Eq. (1). Hence, by combining Eqs. (1) and (2), we obtained $\gamma = w_0/H_r = g\mu_B/\hbar$, namely,

$$hf_r = g\mu_B H_r. \tag{3}$$

It is consistent with the resonance condition ignoring some effects such as the Gilbert damping torque. Based on the above-mentioned result, we obtained the simplified *g*-value combining with the experimental $H_r(\varphi_H)$ to perform some analysis. Here, as for the 30 nm MF-CoFeB thin film, Fig. 3(b) shows an increase in H_r from 673.2 to 754.4 Oe along with an increase in φ_H from 0° to 90°; meanwhile, *g* decreases from 10.44 to 9.32. Next, when φ_H increases from 90° to 180°, H_r decreases from 754.4 to 673.4 Oe, and the corresponding *g*-value increases from 9.32 to 10.44. When φ_H increases from 180° to 360°, there is the next cycle. That is to say, the variation of *g* (Δg) was 1.12, which was bigger than that of OMF-CoFeB ($\Delta g = 0.72$).

There has been the analogous rule in other samples performed, as shown in Table I. Furthermore, *g* is related to spin and orbital angular momentum *S* and *L*,[30]

$$g = 1 + \frac{J(J+1) + S(S+1) - L(L+1)}{2J(J+1)}, \tag{4}$$

where $J = S + L$ is the total angular momentum. Then, we carried out a computation, named partial differential, to obtain the mathematical formula of Δg,

$$dg = \frac{L}{(S+L)^2} dS - \frac{S}{(S+L)^2} dL, \tag{5}$$

where d*g* is consistent with Δg. Considering that the sample is stable, d*S* tends to be 0 so that d*g* is almost inversely proportional to d*L*. As

TABLE I. Angle1 and *g*1 correspond to minimum H_r, angle2 and *g*2 corresponding to maximal H_r, and $\Delta g(=|g1 - g2|)$ in different types of samples.

Sample composition	Angle1 (deg)	*g*1	Angle2 (deg)	*g*2	Δg
Si/Ta 2 nm/OMF-CoFeB 30 nm	0	10.30	90	9.58	0.72
Si/Ta 2 nm/MF-CoFeB 30 nm	0	10.44	90	9.32	1.12
Si/Ta 2 nm/OMF-CoFeB 20 nm	0	9.55	90	8.72	0.83
Si/Ta 2 nm/MF-CoFeB 20 nm	0	10.09	90	8.93	1.16
Copper grid/Ta 2 nm/OMF-CoFeB 10 nm/Ta 2 nm	0	9.25	90	9.08	0.17
Copper grid/Ta 2 nm/MF-CoFeB 10 nm/Ta 2 nm	0	9.32	110	8.86	0.46
Copper grid/MF-CoFeB 10 nm	0	8.93	90	8.24	0.69

a result, ΔL decreases due to the increase in Δg for MF-CoFeB. Then, the orbital magnetic moment m_o is associated with l,[30]

$$\langle m_o^z \rangle = -\frac{\mu}{\hbar} g_l \langle l_z \rangle. \quad (6)$$

It is noted that Eq. (6) belongs to a vector expression. Hence, we can perform a qualitative analysis by using Eq. (6). Here, Δm_o should increase as ΔL decreases, i.e., the higher the value of Δg is, the higher the value of Δm_o will be. Therefore, compared to OMF-CoFeB, it is amorphous MF-CoFeB that had larger Δg and larger variation of orbital magnetic moment Δm_o. All specimens in Table I can also certify this conclusion.

Figures 4(a) and 4(b) show the TEM images (inset) with selected area electron diffraction (SAED) of the sample, and the CoFeB film remains amorphous by the diffused rings in the SAED pattern.[31] Meanwhile, the MF-CoFeB has not observed a distinct difference in the bright field image in comparison with that of OMF-CoFeB [insets of Figs. 4(a) and 4(b)]. However, on these red frame areas of the high-resolution TEM images in Figs. 4(c) and 4(d), the changes in the local atomic structure become visible by Fourier transformation (FT) [Figs. 4(e) and 4(f)] and inverse Fourier transformation (IFT) [Figs. 4(g) and 4(h)]. The OMF-CoFeB formed a few icosahedra-like atomic clusters, which are marked by red circles in Fig. 4(g), and had an arrangement of one atom surrounded by six ones [inset of Fig. 4(g)]. Meanwhile, it seems to be easier to find more icosahedra-like clusters for MF-CoFeB in Fig. 4(h). There is an analogous result in the copper grid substrate in Fig. S1 (see the supplementary material). In addition, after these diffraction patterns have been calibrated with the camera length used and pattern center defined, the diffraction data could be exported along the blue and green lines in Figs. 4(a) and 4(b) to obtain corresponding transmission-electron diffraction pattern (TEDP) in Fig. 4(i). There is a complete second peak although the first peak was hindered by the blocking needle, and it is apparent that the short-range order leads to diffuse Bragg reflections. Meanwhile, compared to OMF-CoFeB, MF-CoFeB has observed the shoulder on the second peak become more marked, which also reflects the increase in icosahedra-like clusters.[14] Interestingly, as shown in Figs. S2 and S3 (see the supplementary material), when performing a series of XPS and EELS analyses, we find electronic intensity at $2p^{1/2}$ and $2p^{3/2}$ energy states of MF-CoFeB significantly stronger than OMF-CoFeB, regardless of Co or Fe element in each scan spot, respectively, which can reflect the Co and Fe atom signals in MF-CoFeB more intensely than OMF-CoFeB, and they further imply that atoms combine into clusters.

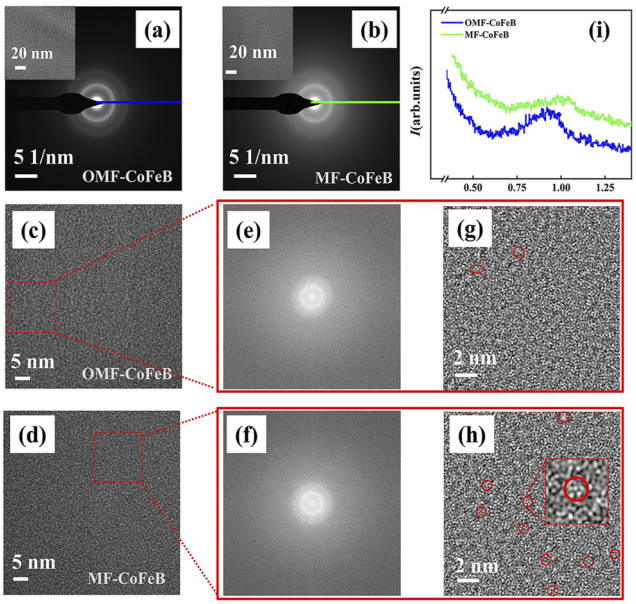

FIG. 4. The selected area diffraction patterns of (a) OMF-CoFeB and (b) MF-CoFeB with the corresponding TEM images (inset). (c) and (d) The high-resolution TEM images and (e)–(h) the corresponding FT and IFT images of the red square area, respectively. (i) Diffraction data corresponding to the green and blue lines in SAED. The thickness of CoFeB thickness is near 30 nm.

Based on the above discussion, we come up with the direction-like order model as shown in Fig. 5 to explain the magnetic field-induced MA in amorphous CoFeB thin film containing two types of ferromagnetic atoms. Figures 5(a) and 5(b) show the models of icosahedral and icosahedra-like clusters observed in Figs. 4(h) and 4(i). Here, the clusters of 12 atoms on icosahedral sites (trigonal or octahedral sites) in Fig. 5(a) [Fig. 5(b)], namely, icosahedral clusters (icosahedra-like clusters), whose top view consists with the arrangement of one atom surrounded by five (six) ones in Figs. 4(h) and 4(i). It is noted that the high-resolution TEM images are still hard to perfectly distinguish between icosahedral and icosahedra-like clusters. Figures 5(c) and 5(d) show the changes of these clusters and the electric cloud state of each atom in OMF-CoFeB and MF-CoFeB, respectively. Compared to these scattered atoms in OMF-CoFeB, when grown CoFeB with an applied magnetic field, atoms combine into clusters and the electron cloud elongates in the direction of magnetization, which is in agreement with the previous report by De Vries *et al.*[32] Furthermore, the state of the outer electron cloud is related to the change in the orbital magnetic moment. By combining with our FMR result, we can surmise that the increase in the orbital magnetic moment is associated with the variation of these atomic clusters in amorphous CoFeB material. In detail, the atomic gathered phenomenon is a benefit to result in orbital hybridization or electron

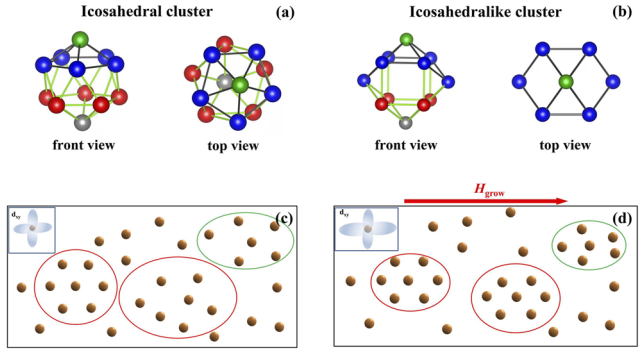

FIG. 5. (a) Icosahedral and (b) icosahedra-like clusters models. The in-plane 2D atom arrangement model with (c) OMF-CoFeB and (d) MF-CoFeB.

cloud orbit elongation with altered orbital angular momentum along the easy axis and further increase in Δm_o.

Therefore, as shown in Figs. 5(c) and 5(d), the direction-like order models can be depicted as follows: On the one hand, more icosahedral and icosahedra-like clusters for MF-CoFeB containing ferromagnetic metal atoms, Co or Fe, at local areas of the amorphous film plane appeared, which increase the order degree. On the other hand, electron cloud may be elongated along H_{grow}, which results in direction-like order in the ferromagnetic property. Hence, we acquire 2D atomic experimental models related to the changes of icosahedral and icosahedra-like clusters in CoFeB thin films, which agrees well with the actual experimental observation and computed results, and explain the magnetic field-induced MA in amorphous CoFeB thin films well.

In summary, amorphous CoFeB ferromagnetic thin films were deposited on Si substrates with the constant magnetic field by dc magnetron sputtering. The thickness dependence of the magnetic properties and the structural properties and the in-plane angular dependence of the resonance field for FMR were mainly investigated. It is more significant for MF-CoFeB films from 10 to 250 nm to observe in-plane uniaxial MA than that of OMF-CoFeB films. Furthermore, this magical phenomenon is related to the strong variation of the g factor, where MF-CoFeB rotated at a different in-plane angle compared to the direction of the easy axis by FMR characterization. In addition, a corresponding increase in the amounts of icosahedral and icosahedra-like clusters was observed by TEM characterization. These results can be commendably explained by the proposed direction-like order model.

See the supplementary material for the other high-resolution TEM images and XPS and EELS results for OMF-CoFeB and MF-CoFeB in the copper grid or the Si substrate.

ACKNOWLEDGMENTS

This work was supported by the National Natural Science Foundation of China (Grant Nos. 51871232, 51871233, and 51931011) and the K. C. Wong Education Foundation (Grant No. GJTD-2020-11).

AUTHOR DECLARATIONS

Conflict of Interest

The authors have no conflicts to disclose.

DATA AVAILABILITY

The data that support the findings of this study are available from the corresponding authors upon reasonable request.

REFERENCES

[1] C. Kittel, Phys. Rev. **71**, 270 (1947).
[2] Y. Liu, B. Wang, Q. Zhan, Z. Tang, H. Yang, G. Liu, Z. Zuo, X. Zhang, Y. Xie, X. Zhu, B. Chen, J. Wang, and R.-W. Li, Sci. Rep. **4**, 6615 (2014).
[3] L. Tauxe, H. N. Bertram, and C. Seberino, Geochem., Geophys., Geosyst. **3**, 1 (2002).
[4] A. I. M. Banderas, A. Aires, F. J. Teran, J. E. Perez, J. F. Cadenas, N. Alsharif, T. Ravasi, A. L. Cortajarena, and J. Kosel, Sci. Rep. **6**, 35786 (2016).
[5] S. Ikeda, K. Miura, H. Yamamoto, K. Mizunuma, H. D. Gan, M. Endo, S. Kanai, J. Hayakawa, F. Matsukura, and H. Ohno, Nat. Mater. **9**, 721 (2010).
[6] O. Idigoras, A. K. Suszka, P. Vavassori, P. Landeros, J. M. Porro, and A. Berger, Phys. Rev. B **84**, 132403 (2011).
[7] X. Chen, B. Wang, X. Wen, P. Sheng, D. Pravarthana, H. Yang, Y. Xie, H. Liu, X. Xu, and R.-W. Li, J. Magn. Magn. Mater. **505**, 166750 (2020).
[8] X. Qiao, X. Wen, B. Wang, Y. Bai, Q. Zhan, X. Xu, and R.-W. Li, Appl. Phys. Lett. **111**, 132405 (2017).
[9] B. D. Cullity and C. D. Graham, *Introduction to Magnetic Materials* (Wiley/IEEE Press, Piscataway, 2009), p. 340.
[10] E. A. Weiss, ACS Nano **15**, 3568 (2021).
[11] B. Liu, B. Wang, T. Nie, Y. Xie, H. Yang, G. Li, J. Pan, and R.-W. Li, Appl. Phys. Lett. **118**, 252404 (2021).
[12] B. Rana, Y. Fukuma, K. Miura, H. Takahashi, and Y. C. Otani, Appl. Phys. Lett. **111**, 052404 (2017).
[13] P. Bruno, Phys. Rev. B **39**, 865 (1989).
[14] G. Suran, K. Ounadjela, and F. Machizaud, Phys. Rev. Lett. **57**, 3109 (1986).
[15] D. H. Shin, H. Niedoba, and G. Suran, IEEE Trans. Magn. **37**, 1422 (2001).
[16] F. Machizaud, K. Ounadjela, and G. Suran, Phys. Rev. B **40**, 587 (1989).
[17] K. Chen, H. Hegde, and F. J. Cadieu, Appl. Phys. Lett. **61**, 1861 (1992).
[18] B. Liu, L. Yang, X. Ruan, J.-W. Cai, L. He, H. Meng, J. Wu, and Y. Xu, New J. Phys. **21**, 053032 (2019).
[19] H. Yamamoto, J. Hayakawa, K. Miura, K. Ito, H. Matsuoka, S. Ikeda, and H. Ohno, Appl. Phys. Express **5**, 053002 (2012).
[20] M. C. Contreras, M. Rivas, I. Iglesias, and J. A. Corrales, IEEE Trans. Magn. **29**, 3885 (1993).
[21] S. U. Jen, T. Y. Chou, and C. K. Lo, Nanoscale Res. Lett. **6**, 468 (2011).
[22] J. Slonczewski, IEEE Trans. Magn. **4**, 15 (1968).
[23] N. Chowdhury and S. Bedanta, AIP Adv. **4**, 027104 (2014).
[24] K. Ounadjela, G. Suran, and F. Machizaud, Phys. Rev. B **40**, 578 (1989).
[25] X. Wen, B. Wang, P. Sheng, S. Hu, H. Yang, K. Pei, Q. Zhan, W. Xia, H. Xu, and R.-W. Li, Appl. Phys. Lett. **111**, 142403 (2017).
[26] Z. Tang, H. Ni, B. Lu, M. Zheng, Y.-A. Huang, S.-G. Lu, M. Tang, and J. Gao, J. Magn. Magn. Mater. **426**, 444 (2017).
[27] A. Gayen, R. Modak, A. Srinivasan, V. V. Srinivasu, and P. Alagarsamy, J. Vac. Sci. Technol. A **37**, 031513 (2019).
[28] M. Büttiker, Phys. Rev. B **27**, 6178 (1983).
[29] C. Kittel, Phys. Rev. **73**, 155 (1948).
[30] J. Stöhr and H. C. Siegmann, *Magnetism: From Fundamentals to Nanoscale Dynamics* (Springer, Stanford, 2006), p. 66.
[31] L. Kipgen, H. Fulara, M. Raju, and S. Chaudhary, J. Magn. Magn. Mater. **324**, 3118 (2012).
[32] G. De Vries, Physica **25**, 1211 (1959).